



## Self-organization of ferroelectric domains induced by water and reinforced via ultrasonic vibration

Shuo Yan<sup>1</sup>, Xueli Hu<sup>1</sup>, Xiaomei Lu<sup>1</sup>  <sup>✉</sup>, Junting Zhang<sup>2</sup> , Xiaofan Shen<sup>1</sup> & Fengzhen Huang<sup>1</sup>  <sup>✉</sup>

Pattern formation caused by self-organization is a fascinating phenomenon that appears in biological, chemical, and physical systems. In ferroelectrics, although a variety of domain patterns have been reported at different scales and dimensions, the self-organization process of ferroelectric domains was rarely investigated. Here, in  $0.72\text{Pb}(\text{Mg}_{1/3}\text{Nb}_{2/3})\text{O}_3-0.28\text{PbTiO}_3$  bulk crystals exposed to water, the self-organized formation process of domain structures is observed and reinforced by ultrasonic vibration. By combining experimental observations and theoretical analysis, we find that adsorbed  $\text{H}^+/\text{OH}^-$  ions on the sample surface act as screening charges to induce the coarsening of the ferroelectric domains. Meanwhile, interactions among dipoles determine the ordering of the domain configuration, while ultrasonic vibration reduces the barrier height for polarization switching. The process of domain evolution deviates from that of the non-conservative dynamic system, and instead fits a percolation model with a clear transition point. This work demonstrates the self-organization of ferroelectric domains induced by water, which is of value for understanding domain dynamics and for the development of high-performance ferroelectric materials.

<sup>1</sup>National Laboratory of Solid State Microstructures and Physics School, Nanjing University, Nanjing 210093, PR China. <sup>2</sup>School of Physical Science and Technology, China University of Mining and Technology, Xuzhou 221116, PR China. ✉email: [xiaomeil@nju.edu.cn](mailto:xiaomeil@nju.edu.cn); [fzhuang@nju.edu.cn](mailto:fzhuang@nju.edu.cn)

The self-organization is a process with only energy input but not external commands. In this process, the intricate and orderly patterns are generated through simple interactions among a large number of components in a system<sup>1,2</sup>. Self-organization is ubiquitous in biology, material science, and chemistry, ranging from molecular to centimeter scales, and exhibiting rich and diverse phenomena, such as material crystallization events in physicochemical systems<sup>3–6</sup>.

Ferroelectrics, as a widely used functional material in sensors, information storage, light modulation, etc., is composed of domains with differently oriented polarization<sup>7–10</sup>. It has long been recognized that the size and configuration of domains are crucial to the performance of ferroelectric materials<sup>11</sup>. In order to improve existing performance and explore novel properties of ferroelectrics, in recent years, domain engineering has become a research hotspot<sup>12–15</sup>. In this respect, the self-organization process of ferroelectric domain, free from any external instructive field but requiring low energy consumption, deserves attention. Although some spontaneously formed domain patterns have been observed, such as the dendrite domain patterns in LiNbO<sub>3</sub> crystal and regular domains in BiFeO<sub>3</sub>(BFO) films<sup>16–19</sup>, in general, self-organization in ferroelectric, especially, the experimental studies of the self-organized domain evolution process were rarely reported.

Ferroelectrics is a kind of solid matter and a thermodynamic system, in which the polarization states and domain structures are closely related to the external environment<sup>20,21</sup>. When ferroelectric materials are placed in a liquid environment, changes in the polarization distribution may occur due to the discontinuity of the intrinsic polarization at the solid-liquid interface. Experimentally, it was observed that ion adsorption from a solution environment led to a polarization reversal in BFO films and in van der Waals layered ferroelectric CuInP<sub>2</sub>S<sub>6</sub><sup>22,23</sup>. Theoretically, it was indicated that water molecules on the surface could induce the reorientation of domains in BFO films, and positive/negative charges on the surface could stimulate the nucleation and growth of reverse domains in PbZr<sub>0.2</sub>Ti<sub>0.8</sub>O<sub>3</sub> films<sup>24,25</sup>. These works mainly focused on low-dimensional ferroelectrics, while for ferroelectric bulk crystals, the solid-liquid interface was rarely

considered to affect the polarization state and the domain configuration<sup>20</sup>. Some recent studies have demonstrated that humidity would affect the shape and size of the domains formed by a scanning tip in LiNbO<sub>3</sub> crystals<sup>26,27</sup>. This phenomenon was attributed to the interplay between polarization switching and screening charge dynamics, and suggested that the presence of water in the environment could influence polarization switching under an electric field. While water did not directly modulate crystal polarization, the findings raised intriguing possibilities for further exploration.

Here we demonstrate a self-organization process of domains in ferroelectric bulk crystals, which is induced by water environment and further positively reinforced by ultrasound. A systematic investigation reveals that the domain evolution process fits the percolation model, and the kinetic character is similar to that with conserved order parameters. This work is of great value for the regulation of domains and the application of ferroelectric materials.

## Results and discussion

### Water-induced self-organization of ferroelectric domains.

Commercial [001]-oriented rhombohedral 0.72Pb(Mg<sub>1/3</sub>Nb<sub>2/3</sub>)O<sub>3</sub>–0.28PbTiO<sub>3</sub>(PMN-28PT) crystals with spontaneous polarization along eight <111> directions are selected as the samples, and the initial samples are composed of irregularly-shaped condensed domains with a 100 nm average size<sup>28</sup>. When the crystals are exposed to water, the domain configuration changes gradually (Fig. 1a). With time increasing, there are two features as shown in Fig. 1b and Fig. 1c. First, the coarsening of domains with the average domain size increases while the domain wall density decreases. Second, the ordering of domains with the domain walls elongating along the in-plane <11> directions. Note that the Piezoresponse Force Microscopy (PFM) images in Fig. 1b were measured at the same position determined by the topography (Supplementary Fig. 1), and the PFM measurements did not induce any change in the domain structure (Supplementary Fig. 2). What's more, the topography did not show any change (Supplementary Fig. 1), indicating that the water treatment did not lead to any degradation of the sample surface<sup>29</sup>. We would

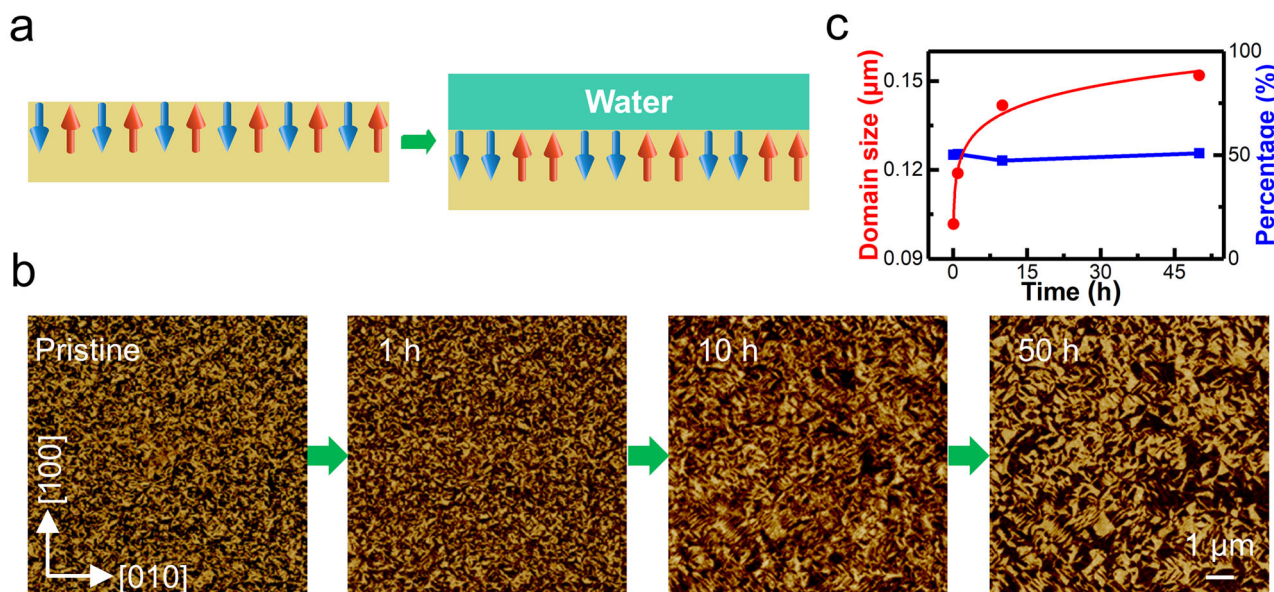


**Fig. 1** Water-induced self-organization of ferroelectric domains. **a** Schematics of the polarization switching after exposing the PMN-28PT crystals to water. The red and blue arrows represent the upward and downward polarization, respectively. **b** Time evolution of PFM images. **c** Time dependence of the average domain size (red) and the area ratio of upward domains (blue) calculated from (b). All PFM images in (b) were measured at the same position of the sample (determined by the topography).

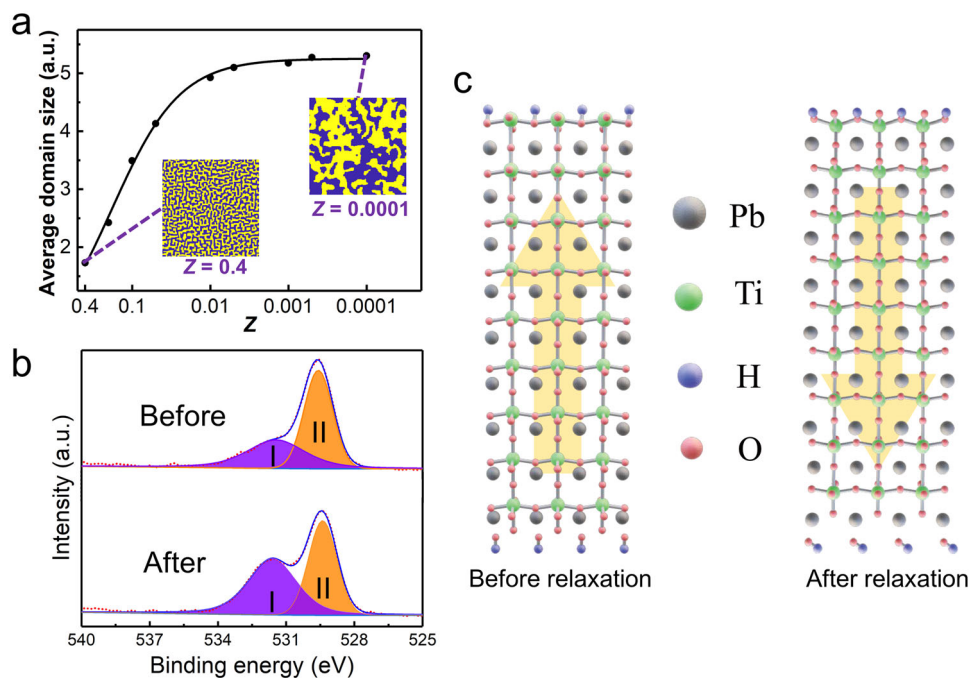


**Fig. 2 Mechanism of water-induced domain evolution.** **a** Average domain size versus unscreened ratio  $Z$  for the 2D Monte Carlo simulation on  $200 \times 200$  lattices. The snapshots are obtained at  $Z = 0.4$  and  $Z = 0.0001$  respectively. Yellow and blue regions represent upward and downward domains, respectively. **b** XPS O 1s core-level spectra for the PMN-28PT crystals before and after water treatment. Peak I centered at 531.4 eV is ascribed to hydroxyl groups chemically bound to surface cations, while Peak II centered at 529.1 eV corresponds to the lattice oxygen. **c** First-principles calculations on the polarization switching in  $\text{PbTiO}_3$  induced by the adsorption of  $\text{H}^+/\text{OH}^-$  ions.

like to mention that such water-induced changes in domains are reproducible (Supplementary Fig. 3).

It is known for the ferroelectric materials that, the discontinuity of spontaneous polarization results in bound charges at the surface/interface and the corresponding depolarization field in the bulk. To stabilize the ferroelectric phase, one way is to form the ferroelectric domains, and another way is to introduce surface screening charges<sup>30</sup>. That is to say, domain formation and surface screening are competing in order to reach obtaining low-energy states.

To explore the effect of screening charges on ferroelectric domains, the Monte Carlo Simulation is employed to study the ferroelectric system with long-range Coulomb interactions and short-range neighbor dipole interactions<sup>31–33</sup>. The Monte Carlo simulation is performed on a 2D  $200 \times 200$  lattice with periodic boundary conditions (see details in Methods). For the initial configuration at high temperature, the square lattice is set with a randomly distributed equal proportion of up and down polarization. As shown in Fig. 2a, with the decrease of  $Z$  (ratio of unscreened bound charges), the size of the simulated domains increases. In other words, as the screening charge increases, the inhibition of domain growth from the long-range effect weakens, and the domains become larger. The picture from the Monte Carlo simulation is consistent with the observed domain coarsening in water (Fig. 1b). Water naturally contains a large amount of  $\text{H}^+$  and  $\text{OH}^-$  ions<sup>22</sup>, and we speculate that these positive and negative charges can be adsorbed onto the surface of PMN-28PT crystals as screening charges, inducing the polarization switching and the corresponding domain growth.

To test our hypothesis, X-ray Photoelectron Spectroscopy (XPS) was used to characterize the sample surface before and after water treatment<sup>29</sup>. As shown in Fig. 2b, the increase of the peak area at the binding energy of 531.4 eV indicates the increase of terminal hydroxyl groups ( $\text{M}-\text{OH}$ )<sup>22</sup>. That means, more  $\text{OH}^-$  ions are adsorbed on the sample surface after water treatment.

This result confirms that the adsorption of ions on the crystal surface is the reason for the coarsening of ferroelectric domains in water.

Density functional theory (DFT) was employed to further investigate the interaction between polarization and  $\text{H}^+/\text{OH}^-$  ions in water at the atomic level. To avoid complicated calculations on PMN-PT solid solution, here we study a simple perovskite structure of  $\text{PbTiO}_3$ , which facilitates the determination of basic physical properties<sup>34</sup>. As shown in Fig. 2c, when  $\text{H}^+$  and  $\text{OH}^-$  ions are adsorbed on the upper positive surface and lower negative surface, respectively, the cations ( $\text{Pb}^{2+}$ ,  $\text{Ti}^{4+}$ ) move from above to below the horizontal O planes, corresponding to a polarization switching from upward to downward.

In addition to domain coarsening, another important feature of domain evolution in water is the ordering of the domain structure (Fig. 1b). The domain walls tend to extend in two specific directions. To display that the ordering is a spontaneous behavior, the domain distribution is statistically analyzed. As shown in Fig. 1c, after 50 h in water, although the average domain size increases from the initial 100 nm to 150 nm, the area ratio of the upward to downward domains remains around 1:1, showing no priority. Such a “free” domain growth without a dominant polarization direction is consistent with the non-commanding external environment we provide. During the water treatment, no external field (such as an electric field) was applied, and the positive and negative ions in the water were “naturally” adsorbed on the crystal surface. Therefore, the ordered domain structure has nothing to do with external command but originates from the self-organization in the ferroelectric system.

We know that self-organization is the spontaneous emergence of ordered collective patterns driven by the interactions among abundant individual components. Here the self-organized domain evolution in Fig. 1b is driven by the interactions among allowed polarizations (dipoles) in the PMN-28PT crystals, and water provides a proper external environment for this process.

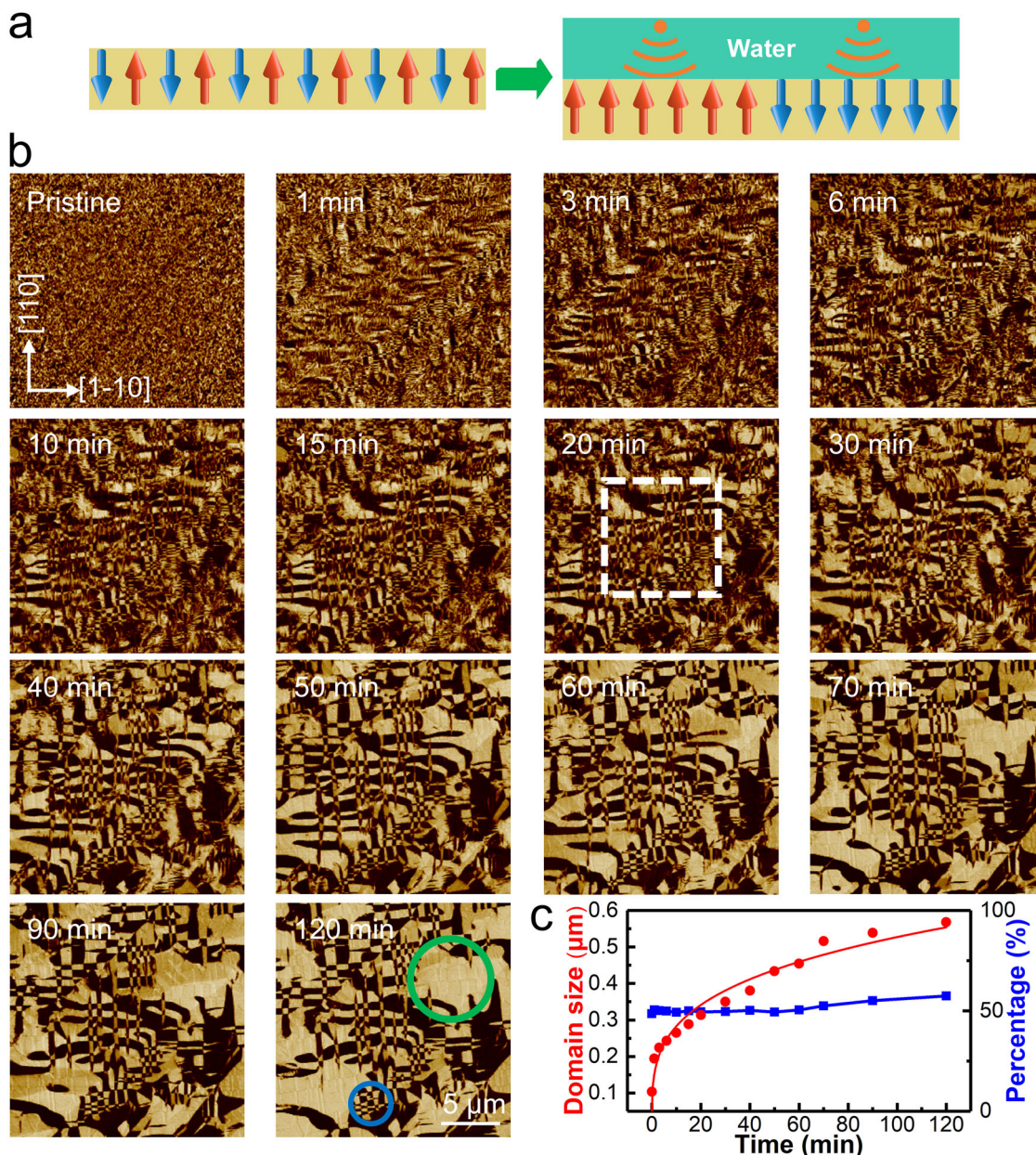


**Fig. 3 Positive reinforcement of the domain self-organization process by ultrasonic vibration.** **a** Schematics of the polarization switching for the PMN-28PT crystals in water with ultrasound. **b** Time evolution of PFM images. The white dotted box demarcates the measurement area of the high-resolution PFM. Additionally, the green and blue circles indicate domains greater than  $20 \mu\text{m}^2$  and less than  $1 \mu\text{m}^2$ , respectively. **c** Time dependence of the average domain size (red) and the area ratio of upward domains (blue) calculated from (b).

It should be noted that, in any case, the emergence of ordered domain pattern is determined by the minimum energy of the ferroelectric system<sup>11</sup>, including electrostatic energy, elastic energy, etc.

#### Self-organization positively reinforced by ultrasonic vibration.

The growth of the domains in water is rather slow, and the average domain size only increased to 150 nm after 50 h. To better understand the self-organization behavior, ultrasonic vibration is used to accelerate the domain growth (Fig. 3a).

When PMN-28PT crystals were exposed to water with ultrasound (40 kHz, 50 W), the domain structure changed drastically (Fig. 3b, c). Significant changes in the domain structure can be observed in just 1 min, and the domain size after 10 min exceeds that after 50 h in still water (Fig. 1b).

At 120 min, the average domain size is about  $0.6 \mu\text{m}$  with the largest domain reaching  $6 \mu\text{m}$ . Along with the domain coarsening, the configuration of the domains becomes much more ordered with many elongated domain walls in the in-plane  $\langle 11 \rangle$  direction.

All PFM images in Fig. 3b were acquired at the same location and determined by the topography (Supplementary Fig. 4). We also provide the corresponding PFM amplitude images in Supplementary Fig. 5. With the time (average domain size) increasing, the average amplitude over the measured area also increases. In addition, X-ray diffraction (XRD, Bruker D8 Advance, Cu K $\alpha$  rays) measurements were performed on PMN-28PT crystals before and after treatment (exposed to water with ultrasound for 120 min). As shown in Supplementary Fig. 6, the domain changes are not accompanied by a phase transition, and the crystal remains in the rhombohedral phase.

The water-induced self-organized domain structure was quite stable, and no change was observed after the sample was kept in atmosphere for a long time (Supplementary Fig. 7). This is also the key point of the self-organization process, that is, although the formation of ordered domain patterns is driven by the interaction among dipoles, energy input is required from the outside. Once the energy input stops, the self-organization process stops. Based on this special mechanism of domain growth, we were able to record the growth and merge process of ferroelectric domains.

To investigate the domain structure inside the bulk of the crystal, we used the buffered oxide etchant to etch a treated crystal<sup>35</sup>. The results presented in Supplementary Fig. 8 demonstrate that the domain structure remains unchanged up to an etching depth of  $\sim 3 \mu\text{m}$ . Furthermore, confocal second-harmonic microscopy<sup>36</sup> reveals that the domain evolution extends to a depth of at least  $20 \mu\text{m}$  beneath the surface (Supplementary Fig. 9). The water-induced domain evolution is expected to extend to the interior of the crystal. However, it does not necessarily mean that the domains observed on the surface penetrate the entire  $500 \mu\text{m}$  thickness of the crystal, as conclusive evidence for this point is not currently available.

As a comparison to the experiment in Fig. 3, we performed a controlled experiment without water (Supplementary Fig. 10a), and found that ultrasound alone has a limited impact on the domains. Further, with ultrasound (40 kHz, 50 W), we also exposed the samples to alcohol, acidic, and alkaline aqueous solution, respectively. As shown in Supplementary Fig. 10b–d, there is no observable change in domain configuration after 30 min, which means the self-organization process of ferroelectric domains in these solutions are greatly suppressed compared with that in water (Fig. 3b). Ethanol is a non-electrolyte with very few ions, and  $\text{H}^+(\text{OH}^-)$  is dominant in acid (alkaline) solution. The different effects of these solutions and water indicate that abundant and comparable amount of positive and negative ions in water are the cause of domain changes, and ultrasonic vibration plays a role in promoting the self-organization process of domains.

In detail, when the positive and negative ions in water are adsorbed on the polar surface and release the adsorption energy, polarization switching can be induced to enlarge the domains, and the ions further act as screening charges to stabilize the polarization states. Ultrasonic vibration transfers mechanical energy to the interior of the sample, which helps to reduce the potential barrier of ferroelectric/ferroelastic switching and the domain wall motion, to accelerate the growth of domains. Moreover, in the emerging field of piezocatalysis, studies have indicated that ultrasonic waves could promote the formation and collapse of bubbles on the particle surface. The ultrasonic cavitation bubbles that collapse instantaneously will release local electric, mechanical, and thermal fields, which also promote polarization switching<sup>37–39</sup>.

Self-organized growth tends to generate fractal structures, and the core feature of fractals is self-similarity<sup>40,41</sup>. In fact, the self-organized growth of the ferroelectric domains exhibits a self-similarity over time. Figure 4a–c is the evolution of binarized PFM images after different times in water with ultrasound. Figure 4d gives the image taken also for the 120 min-treated samples but with a larger area than that of Fig. 4c. Comparing Fig. 4b with Fig. 4d, similar domain morphologies and distributions were observed. Without a scale bar, it is challenging to differentiate the actual scan size.

The self-similarity behavior can be quantified by the fractal dimension<sup>42</sup>. In this study, we compute the fractal dimension of domain walls ( $D_{dw}$ ) using the box-counting method (Fig. 4e). Our findings (Fig. 4f) demonstrate that for the same observation area (Fig. 4a–c), the  $D_{dw}$  decreases over time, while the  $D_{dw}$  of Fig. 4d

(120 min, scan size  $40 \mu\text{m}$ ) is approximately equal to that of Fig. 4b (30 min, scan size  $20 \mu\text{m}$ ), indicating the self-similarity in a statistical sense. The self-similarity further confirms the self-organization nature of the domain evolution process.

**Dynamics analysis on the self-organization process.** For the continuous evolution of the ferroelectric domain structure, the dynamic process is usually characterized by the correlation length as the function of time  $L(t)$ <sup>43</sup>. Firstly, the spatial correlation function  $C(r, t) = \langle S(r, t)S(0, t) \rangle$  is calculated, where  $t$  is time,  $r$  is the position of a point in a domain,  $S(r, t)$  represents the scalar order parameter field with +1 and -1 for  $r$  inside an upward and downward domain respectively, and the brackets denote the spatial average. Then,  $L(t)$  can be extracted, defined as the distance where  $C(r, t)$  drops to half of  $C(0, t)$ . The temporal variation of  $L(t)$  used to be described with a power-law dependence  $L(t) \propto (t - t_0)^n$ , where  $t_0$  is a constant offset time and  $n$  is the growth exponent characterizing the rate of domain coarsening<sup>44,45</sup>.

The calculated and corresponding fitting results are shown in Fig. 5a. Two universality classes of growth exponent are well understood, with  $n = 1/2$  and  $n = 1/3$  corresponding to systems with non-conservative and conservative order parameters, respectively<sup>46</sup>. In most of the conservative systems, there are heat and mass transport. Taking binary alloys, for example,  $A$  and  $B$  atoms with conserved numbers cannot be converted to each other, and the slow dynamic behavior is related to the diffusion process. On the contrary, upward and downward polarization can be converted into each other, thus ferroelectrics are generally considered to be non-conservative systems with faster dynamic behavior<sup>44</sup>. However, here the fitting exponent  $n$  for the self-organized domain evolution in water with ultrasound is 0.3, far from that of the non-conservative system, but very close to the conservative system.

This deviation is understandable. During the domain self-organization process, there is no command (such as the electric field) from outside. Although the upward and downward polarizations can be reversed to each other, the area ratio of positive to negative domains is always close to 1:1. Thus, the ferroelectrics in water can be analogized in a sense to the binary alloys with conserved  $A$  and  $B$  atom numbers. To put it another way, the deviation from the dynamic behavior of the non-conservative system also confirms that the self-organization shown here is different from the general dynamics of domain growth.

**Percolation analysis on the self-organization process.** Although we can see easily from Fig. 3b that, with time elapse, the average domain size increases, and the domain walls tend to grow in specific direction, the evolution process of the domain configuration is much more complicated. The size, shape, and change of each domain are different. For example, large domains appear after a long time, such as domains over  $20 \mu\text{m}^2$  at 120 min (Fig. 3b, green circle), there are also small domains interspersed, even less than  $1 \mu\text{m}^2$  (Fig. 3b, blue circle). In short, the evolution of the domains is far from uniform. Such a special process can hardly be analyzed by conventional tracking or averaging methods. On the one hand, tracking one single domain is not enough to fully express the evolutionary process; on the other hand, statistical averaging can easily erase the diversity of changes.

The percolation model is widely applied to describe dynamic phenomena for a broad range of topics in physics, materials science, complex networks, epidemiology<sup>47–49</sup>. To combine the overall organization and details of domains, the percolation model is used to analyze the self-organization process of ferroelectric domains.

For the percolation analysis, firstly, a region in the white dashed square in Fig. 3b was measured by PFM with higher

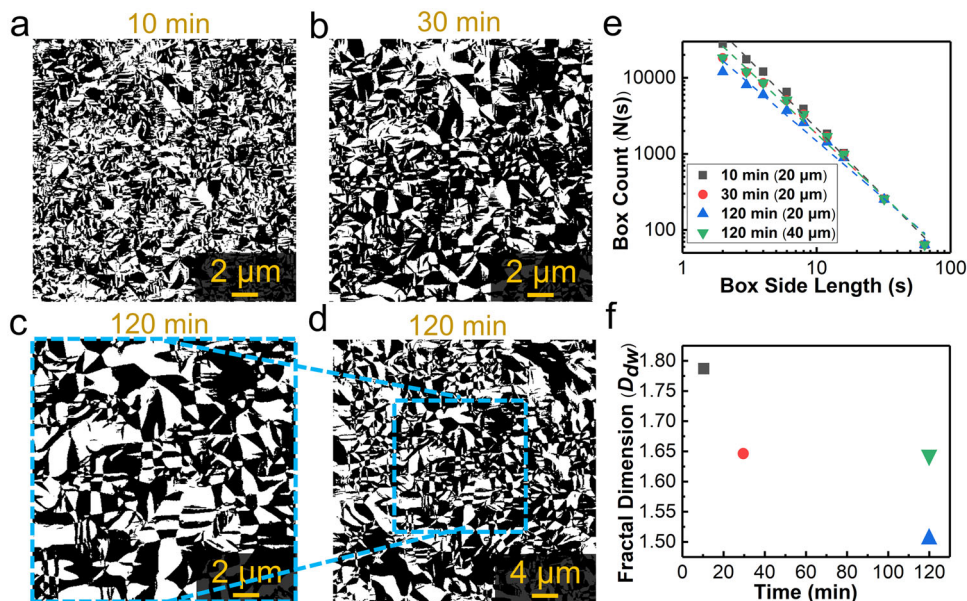


**Fig. 4 Self-similar growth of the domains.** Binarized PFM images of the PMN-28PT crystal after (a) 10 min, (b) 30 min, and (c, d) 120 min in water with ultrasound, with white and black represent upward and downward polarization, respectively. a–c are measured at same area, while (d) is measured at a 4-times larger area including that of (c). e Linear regression of the box count vs box side length in the box-counting method for the fitting of fractal dimension, which corresponds to the absolute value of the slope. f Plot of fractal dimensions over time.

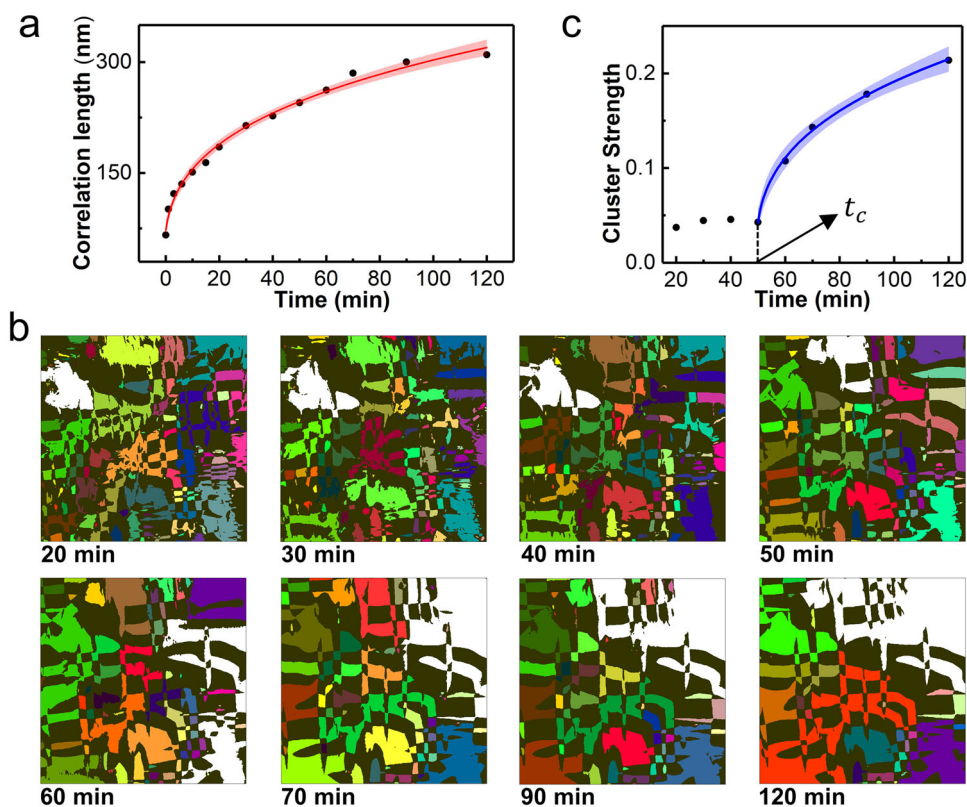


**Fig. 5 Theoretical analysis of the self-organization process in PMN-28PT crystals.** a Time evolution of the correlation length  $L(t)$  for dynamic analysis. b Processed PFM images from Supplementary Fig. 11 for percolation analysis, with different colors representing different clusters, and the white color indicates the largest cluster in each image. c Dependency of the cluster strength  $P_\infty$  on time.

spatial resolution, covering 20 min to 120 min, and the results are shown in Supplementary Fig. 11. Then, the PFM image in Supplementary Fig. 11 was processed (see Methods for details) to present as a combination of clusters (Fig. 5b), where different colors represent different clusters (connected regions), with the

largest cluster marked in white. In general, the average size of the clusters increases with time. Particularly, the size of the white cluster shows almost no change below 50 min, while at 60 min, the white cluster enlarges significantly, connecting the right and the bottom edges. For quantitative analysis, the cluster strength is

defined as  $P_\infty = n_\infty/N^{50}$ , where  $n_\infty$  is the number of pixels that belong to the biggest cluster and  $N$  is the total number of pixels in the processed PFM image. Figure 5c gives cluster strength  $P_\infty$  versus time with a special moment  $t_c$ . Below  $t_c$ ,  $P_\infty$  is almost unchanged, while above  $t_c$ , the data can be fitted by  $(t - t_c)^\beta$ , with  $\beta = 0.35$  and  $t_c = 49.3$  min. This signals the existence of a percolative transition at  $t_c$ , when the largest cluster extends from one boundary to another.

It is reported that the percolation phenomenon could be induced by the dc electric field in KTN:Li crystals at low temperature<sup>51</sup>. In contrast, what we observed here is a self-organized behavior with non-commanding external energy provided by either ion in water or ultrasonic vibration. The water-induced evolution of domain configuration with time is somewhat similar in form to the gelation of colloids after introducing salts<sup>52</sup>, with percolation as the process feature and a large-scale ordered pattern as the final result.

It is known that domain configuration is closely associated with the performance of ferroelectric materials. Here we simply demonstrate the effect of domain configuration on the electric hysteresis characters (Polarization-Voltage). As shown in Supplementary Fig. 12, with most of the domains in the samples evolving from uniform, disordered, and isolated small ones to irregular, ordered, and related large ones, the increase of polarization with applied voltage slows down. We try to understand the shape of the hysteresis loops based on the variant threshold voltage of each domain related to the domain size, which is expected to be larger for larger domains<sup>53,54</sup>. In sample S (treated for 5 min), the size and the threshold voltage of different domains are similar. While in sample L (treated for 120 min), the size and the threshold voltage of different domains exhibit a significant range of variation, resulting in a distribution in the switching threshold of different domains. As the applied voltage increases, the domains in sample L might reverse gradually starting from smaller ones, leading to a slow increase in the macroscopic polarization. Although the domain structure is considered to dominate the ferroelectric hysteresis behavior, it should be noted that ferroelectric switching can be affected by many factors. Here we cannot discount the possibility that defects may form during the water treatment process, which may also contribute to the changes in hysteresis loops through pinning.

In the end, we perform a discussion of our work and that of others on low-dimensional materials. For low-dimensional material<sup>22,23,29</sup>, an initial polarization direction is present, either upward or downward. Positive and negative charges preferentially adsorb on surfaces with initial upward and downward polarizations, respectively, resulting in a polarization reversal from upward to downward or vice versa. However, in the PMN-28PT crystal, we investigated, there is no specific initial polarization direction in the crystal. The area ratio of the upward to downward domains is around 1:1. When the crystal is immersed in water, a non-instructive environment with comparable numbers of positive and negative ions, polarization switching occurs with equal probabilities in the upward and downward directions, leading to the self-organized growth of domains driven by the system's total energy. Throughout the evolution process, the proportion of upward and downward polarization areas remains roughly equal.

## Conclusions

Although the effect of ion adsorption on the domain structure has been discovered and studied in ferroelectric thin films and 2D ferroelectric materials, that on ferroelectric crystals was always considered negligible. In this work, we report the self-organization of domains in PMN-28PT crystals can be induced by water and positively enhanced by ultrasonic vibration. The adsorption of

$H^+/OH^-$  ions induces polarization switching and domain growth, which tends to be ordered due to the interaction among the dipoles. The ultrasonic vibration reduces the barrier of polarization switching and reinforces the domain self-organization process. A careful analysis reveals a slow dynamic behavior of the domain growth, and the domain self-organization process conforms to the percolation model with a distinct transition moment. This work provides important information for the understanding of domain dynamics and the modulation of ferroelectric materials.

## Methods

**Sample preparation.** Commercial [001]-oriented rhombohedral PMN-28PT crystals were selected as the samples. Since the samples were mechanically polished to a thickness of 500  $\mu\text{m}$ , to minimize the influence of internal stress, a thermal annealing process was applied to the crystals. The samples were annealed at 300  $^\circ\text{C}$  for 2 h and then naturally cooled to room temperature. For the water treatment: The PMN-28PT crystals were treated with deionized water at room temperature in a 25 mL beaker. The inner diameter and the height of the beaker were 3.2 cm and 5.5 cm, and the height of deionized water was 3 cm. The beaker was sealed and placed on a stationary desktop during the water treatment. For the water treatment with ultrasonic vibration: The above beaker containing a crystal was suspended within the ultrasonic bath and sonicated (40 kHz, 50 W). The height of water in the ultrasonic bath was about 7 cm.

**PFM measurement.** Commercial atomic force microscopy (Bruker, Icon) was used to measure the ferroelectric polarization of the sample, with the Pt/Ir-coated Si tip (SCM-PIT-V2), 0.5 Hz scan rate, 200 mV drive amplitude, and 370 kHz drive frequency. The ferroelectric domains were characterized under the Vertical PFM mode, and all the PFM images given in Fig. 1 and Fig. 3 are out-of-phase images. After the water treatment and before the PFM characterization, the crystals were dried with an  $N_2$  gun for about 5 s at room temperature.

**Monte Carlo simulation.** Considering long-range Coulomb interactions and short-range neighbor dipole interactions, the Hamiltonian of the system can be expressed as:

$$H = H_{short} + H_{long} = -J \sum_{\langle i,j \rangle} P_i P_j + \sum_{i,j} \frac{Z^2 q_i q_j}{\epsilon_r r_{ij}} \quad (1)$$

The first and second terms represent the short-range dipole-dipole interaction and the long-range charge-charge interaction, respectively. On each lattice site  $i$ , an electric dipole  $P_i$  is imposed, with  $P_j$  set to +1 and -1 for upward and downward polarization, respectively.  $J$  is the interaction between neighboring dipoles  $P_i$  and  $P_j$ . The bound charges  $q_i$  are set to +1 and -1 with upward and downward polarization on each site, respectively.  $Z$ , in the range of 0-1, represents the ratio of unscreened bound charges on each lattice site, with  $Z = 0$  for full-screen conditions.  $\epsilon_r$  is the relative permittivity, and  $r_{ij}$  is the distance between sites  $i$  and  $j$ . For simplicity, we set  $J = 1$  and  $\epsilon_r = 1$ .

**First-principles calculations.** The first-principles calculations based on DFT were performed using the projector-augmented wave method<sup>55</sup>, as implemented in the Vienna Ab Initio Simulation Package<sup>56</sup>. The Perdew-Burke-Ernzerhof functional modified for solids was used as the exchange-correlation functional<sup>57</sup>. Nine perovskite layers were used to model the  $\text{PbTiO}_3$  bulk with  $\text{PbO}$  and  $\text{TiO}_2$  terminal surfaces. Due to the periodic condition, a vacuum space of 15  $\text{Å}$  was used in the supercell to separate the neighboring images along the vertical axis. A cutoff energy of 550 eV was used for the plane wave expansion, and a G-centered  $9^*9^*1$  k-point mesh was used for the Brillouin zone integration. The lattice parameters and internal atomic coordinates were relaxed until the Hellman-Feynman force on each atom was less than 0.05 eV/ $\text{Å}$ , and a convergence threshold of  $10^{-6}$  eV was used for the electronic self-consistency loop. The adsorption energies of  $H^+$  and  $OH^-$  ions at different locations on the crystal surface were calculated. The  $H^+$  ions tend to be adsorbed near O ions, while  $OH^-$  ions are near Pb (Ti) ions, resulting in changes in the local polarization state. Nevertheless, in the case of upward (downward) polarization, when the  $H^+$  ( $OH^-$ ) ions bond with O (Ti) ions on the upper surface while  $OH^-$  ( $H^+$ ) ions bond with Pb (O) ions on the lower surface, the polarization switching could occur in a large range.

**XPS measurement.** XPS was recorded by Thermo ESCALAB 250XI equipped with an Al  $K_\alpha$  X-ray source at ambient temperature and a chamber pressure of about  $8 \times 10^{-10}$  Pa. The X-ray gun was operated at 16 mA and 12.5 kV. All the spectra were corrected by setting the reference binding energy of carbon (C1s) at 284.80 eV.

**Preprocessing for percolation analysis.** To delineate the percolative region, we first binarize the PFM images, with a pixel considered to be in state 1 if it has an upward polarization and in state 0 for downward polarization. To identify the cluster size in

the binarized images, we define connected pixels that make up a cluster using the Von Neumann neighborhood criterium: square-shaped pixels are considered connected when they share the binarized state along an edge, while pixels that share a vertex, i.e., are adjacent and have the same state along the diagonal of the pixel lattice, are not considered connected. With time increasing, the number, the size, and the shape of the clusters undergo changes, making it difficult to track and assign the same color to each region. Hence, MATLAB was utilized to color the clusters automatically, with the largest cluster specified in white.

### Data availability

The authors declare that all the data supporting the conclusion of the present study are available within the paper and supporting information and also from the corresponding author upon reasonable request.

Received: 22 November 2022; Accepted: 17 May 2023;

Published online: 26 May 2023

### References

- Camazine, S., et al. *Self-Organization in Biological Systems* (Princeton University Press, 2003).
- Haken, H. *Information and Self-Organization: A Macroscopic Approach to Complex Systems* (Springer 2006).
- Whitesides, G. M. & Boncheva, M. Beyond molecules: Self-assembly of mesoscopic and macroscopic components. *Proc. Natl. Acad. Sci.* **99**, 4769–4774 (2002).
- Mahadevan, L. & Rica, S. Self-organized origami. *Science* **307**, 1740 (2005).
- Cross, M. C. & Hohenberg, P. C. Pattern formation outside of equilibrium. *Rev. Mod. Phys.* **65**, 851–1112 (1993).
- Rietkerk, M. & van de Koppel, J. Regular pattern formation in real ecosystems. *Trends Ecol. Evol.* **23**, 169–175 (2008).
- Scott, J. F. Applications of modern ferroelectrics. *Science* **315**, 954–959 (2007).
- Dawber, M., Rabe, K. M. & Scott, J. F. Physics of thin-film ferroelectric oxides. *Rev. Mod. Phys.* **77**, 1083–1130 (2005).
- Lv, L. et al. Reconfigurable two-dimensional optoelectronic devices enabled by local ferroelectric polarization. *Nat. Commun.* **10**, 3331 (2019).
- Zhang, S. et al. Advantages and challenges of relaxor-PbTiO<sub>3</sub> ferroelectric crystals for electroacoustic transducers—a review. *Prog. Mater. Sci.* **68**, 1–66 (2015).
- Scott, J. F. *Ferroelectric Memories* (Springer 2000).
- Qiu, C. et al. Transparent ferroelectric crystals with ultrahigh piezoelectricity. *Nature* **577**, 350–354 (2020).
- Chen, C. et al. Large-scale domain engineering in two-dimensional ferroelectric CuInP<sub>2</sub>S<sub>6</sub> via giant flexoelectric effect. *Nano Lett.* **22**, 3275–3282 (2022).
- Tian, Y. et al. Large-area printing of ferroelectric surface and super-domain for solar water splitting. *Adv. Funct. Mater.* **32**, 2111180 (2022).
- Liu, Y. et al. Controllable electrical, magnetoelectric and optical properties of BiFeO<sub>3</sub> via domain engineering. *Prog. Mater. Sci.* **127**, 100943 (2022).
- Shur, V. Y. et al. Formation of self-organized domain structures with charged domain walls in lithium niobate with surface layer modified by proton exchange. *J. Appl. Phys.* **121**, 104101 (2017).
- Chae, S. C. et al. Self-organization, condensation, and annihilation of topological vortices and antivortices in a multiferroic. *Proc. Natl. Acad. Sci.* **107**, 21366–21370 (2010).
- Haykal, A. et al. Antiferromagnetic textures in BiFeO<sub>3</sub> controlled by strain and electric field. *Nat. Commun.* **11**, 1704 (2020).
- Chauleau, J. Y. et al. Electric and antiferromagnetic chiral textures at multiferroic domain walls. *Nat. Mater.* **19**, 386–390 (2020).
- Kalinin, S. V., Kim, Y., Fong, D. D. & Morozovska, A. N. Surface-screening mechanisms in ferroelectric thin films and their effect on polarization dynamics and domain structures. *Rep. Prog. Phys.* **81**, 036502 (2018).
- Nahas, Y. et al. Inverse transition of labyrinthine domain patterns in ferroelectric thin films. *Nature* **577**, 47–51 (2020).
- Tian, Y. et al. Water printing of ferroelectric polarization. *Nat. Commun.* **9**, 3809 (2018).
- Xu, D. D. et al. Ion adsorption-induced reversible polarization switching of a van der Waals layered ferroelectric. *Nat. Commun.* **12**, 655 (2021).
- Li, X., Bai, Y., Wang, B. C. & Su, Y. J. Water adsorption induced in-plane domain switching on BaTiO<sub>3</sub> surface. *J. Appl. Phys.* **118**, 094104 (2015).
- Liu, D., Zhao, R., Jafri, H. M., Wang, J. & Huang, H. Phase-field simulations of surface charge-induced polarization switching. *Appl. Phys. Lett.* **114**, 112903 (2019).
- Ievlev, A. V. et al. Intermittency, quasiperiodicity and chaos in probe-induced ferroelectric domain switching. *Nat. Phys.* **10**, 59 (2013).
- Ievlev, A. V., Morozovska, A. N., Eliseev, E. A., Shur, V. Y. & Kalinin, S. V. Ionic field effect and memristive phenomena in single-point ferroelectric domain switching. *Nat. Commun.* **5**, 4545 (2014).
- Yan, S. et al. Large-scale optical manipulation of ferroelectric domains in PMN-PT crystals. *Adv. Opt. Mater.* **10**, 2201092 (2022).
- Lee, H. et al. Imprint control of BaTiO<sub>3</sub> thin films via chemically induced surface polarization pinning. *Nano Lett.* **16**, 2400–2406 (2016).
- Vorotiahin, I. S. et al. Tuning the polar states of ferroelectric films via surface charges and flexoelectricity. *Acta Mater.* **137**, 85–92 (2017).
- Christiansen, H., Majumder, S., Henkel, M. & Janke, W. Aging in the long-range Ising Model. *Phys. Rev. Lett.* **125**, 180601 (2020).
- Zhang, J. et al. Origin of sawtooth domain walls in ferroelectrics. *Phys. Rev. B* **101**, 060103 (2020).
- Gleiser, P. M., Tamarit, F. A., Cannas, S. A. & Montemurro, M. A. Slow dynamics in a two-dimensional Ising model with competing interactions. *Phys. Rev. B* **68**, 134401 (2003).
- Fu, H. & Cohen, R. E. Polarization rotation mechanism for ultrahigh electromechanical response. *Nature* **403**, 281–283 (2000).
- Hooton, J. A. & Merz, W. J. Etch patterns and ferroelectric domains in BaTiO<sub>3</sub> single crystals. *Phys. Rev.* **98**, 409 (1955).
- Wei, D. et al. Efficient nonlinear beam shaping in three-dimensional lithium niobate nonlinear photonic crystals. *Nat. Commun.* **10**, 4193 (2019).
- Su, R. et al. Nano-ferroelectric for high efficiency overall water splitting under ultrasonic vibration. *Angew. Chemie - Int. Ed.* **58**, 15076 (2019).
- Wang, Y. et al. Piezo-catalysis for nondestructive tooth whitening. *Nat. Commun.* **11**, 1328 (2020).
- Wang, Y. et al. Ultrasonic activation of inert poly(tetrafluoroethylene) enables piezocatalytic generation of reactive oxygen species. *Nat. Commun.* **12**, 3508 (2021).
- Mandelbrot, B. B., *The Fractal Geometry of Nature* (WH Freeman, 1982).
- Takayasu, H. & Inaoka, H. New type of self-organized criticality in a model of erosion. *Phys. Rev. Lett.* **68**, 966 (1992).
- Moran-Mirabal, J. M., Aubrecht, D. M. & Craighead, H. G. Phase separation and fractal domain formation in phospholipid/diacetylene-supported lipid bilayers. *Langmuir* **23**, 10661 (2007).
- Likodimos, V., Orlik, X. K., Pardi, L., Labardi, M. & Allegrini, M. Dynamical studies of the ferroelectric domain structure in triglycine sulfate by voltage-modulated scanning force microscopy. *J. Appl. Phys.* **87**, 443–451 (2000).
- Likodimos, V. et al. Thermally activated ferroelectric domain growth due to random defects. *Phys. Rev. B* **63**, 641041–641044 (2001).
- Gavagnin, E., Owen, J. P. & Yates, C. A. Pair correlation functions for identifying spatial correlation in discrete domains. *Phys. Rev. E* **97**, 062104 (2018).
- Likodimos, V., Labardi, M. & Allegrini, M. Domain pattern formation and kinetics on ferroelectric surfaces under thermal cycling using scanning force microscopy. *Phys. Rev. B* **66**, 024104 (2002).
- Essam, J. W. Percolation theory. *Rep. Prog. Phys.* **43**, 833–912 (1980).
- Lemoult, G. et al. Directed percolation phase transition to sustained turbulence in Couette flow. *Nat. Phys.* **12**, 254–258 (2016).
- Kyrylyuk, A. V. & Van Der Schoot, P. Continuum percolation of carbon nanotubes in polymeric and colloidal media. *Proc. Natl. Acad. Sci.* **105**, 8221–8226 (2008).
- Prosandeev, S., Wang, D., Akbarzadeh, A. R., Dkhal, B. & Bellaiche, L. Field-induced evolution of polar nanoregions in relaxor ferroelectrics. *Phys. Rev. Lett.* **110**, 207601 (2013).
- Falsi, L. et al. Direct observation of fractal-dimensional percolation in the 3D cluster dynamics of a ferroelectric supercrystal. *Phys. Rev. Lett.* **126**, 037601 (2021).
- Tsurusawa, H., Leocmach, M., Russo, J. & Tanaka, H. Direct link between mechanical stability in gels and percolation of isostatic particles. *Sci. Adv.* **5**, eaav6090 (2019).
- Jin, L., Li, F. & Zhang, S. Decoding the fingerprint of ferroelectric loops: comprehension of the material properties and structures. *J. Am. Ceram. Soc.* **97**, 1–27 (2014).
- Liu, S., Grinberg, I. & Rappe, A. M. Intrinsic ferroelectric switching from first principles. *Nature* **534**, 360–363 (2016).
- Blöchl, P. E. Projector augmented-wave method. *Phys. Rev. B* **50**, 17953–17979 (1994).
- Kresse, G. & Furthmüller, J. Efficient iterative schemes for ab initio total-energy calculations using a plane-wave basis set. *Phys. Rev. B* **54**, 11169–11186 (1996).
- Perdew, J. P. et al. Restoring the density-gradient expansion for exchange in solids and surfaces. *Phys. Rev. Lett.* **100**, 136406 (2008).

### Acknowledgements

This work was supported by the National Natural Science Foundation of China (51721001, 11874208, 52172116, 62171214, and 11974418), and the Priority Academic Program Development of Jiangsu Higher Education Institutions (PAPD).



### Author contributions

The work was conceived and designed by S.Y. and X.L.; S.Y. prepared the samples, with assistance from X.H.; S.Y. and X.H. performed the experiments, with assistance from F.H.; X.L. and F.H. supervised the experiments; J.Z. and X.S. performed the DFT calculation; S.Y. performed the Monte Carlo simulations and the Percolation Analysis with the supervision of X.L.; S.Y. and X.H. drafted the manuscript; X.L., J.Z., and F.H. revised the manuscript, and all authors discussed the results.

### Competing interests

The authors declare no competing interests.

### Additional information

**Supplementary information** The online version contains supplementary material available at <https://doi.org/10.1038/s43246-023-00371-6>.

**Correspondence** and requests for materials should be addressed to Xiaomei Lu or Fengzhen Huang.

**Peer review information** *Communications Materials* thanks Dawei Zhang and the other, anonymous, reviewer(s) for their contribution to the peer review of this work. Primary Handling Editors: Andreja Benčan Golob and John Plummer. A peer review file is available.

**Reprints and permission information** is available at <http://www.nature.com/reprints>

**Publisher's note** Springer Nature remains neutral with regard to jurisdictional claims in published maps and institutional affiliations.



**Open Access** This article is licensed under a Creative Commons Attribution 4.0 International License, which permits use, sharing, adaptation, distribution and reproduction in any medium or format, as long as you give appropriate credit to the original author(s) and the source, provide a link to the Creative Commons licence, and indicate if changes were made. The images or other third party material in this article are included in the article's Creative Commons licence, unless indicated otherwise in a credit line to the material. If material is not included in the article's Creative Commons licence and your intended use is not permitted by statutory regulation or exceeds the permitted use, you will need to obtain permission directly from the copyright holder. To view a copy of this licence, visit <http://creativecommons.org/licenses/by/4.0/>.

© The Author(s) 2023